Syntheses and Crystal Structures of Three Copper Tellurides: $BaDyCuTe_3$, $K_{1.5}Dy_2Cu_{2.5}Te_5$, and Acentric $K_{0.5}Ba_{0.5}DyCu_{1.5}Te_3$

Fu Qiang Huang, Wonyoung Choe, Stephen Lee,* and Jacquelyne S. Chu

Department of Chemistry, The University of Michigan, Ann Arbor, Michigan 48109-1055

Received October 27, 1997. Revised Manuscript Received March 2, 1998

Three compounds, $BaDyCuTe_3$, $K_{1.5}Dy_2Cu_{2.5}Te_5$, and $K_{0.5}Ba_{0.5}DyCu_{1.5}Te_3$, were synthesized from the reaction at 850 °C of the pure elements with fluxes such as $BaCl_2$ or a eutectic mixture of LiCl/KCl. The crystal structures of the three compounds were determined by the single-crystal X-ray method. The final *R*-values for the three crystals were, respectively, 4.34%, 3.95%, and 3.46%. All three structures can be viewed as tetrahedral structures based on $CuTe_4$ units. $BaDyCuTe_3$ crystallizes in the orthorhombic space group *Cmcm* (no. 63) with cell dimensions of $a = 4.4286(3)$ Å, $b = 14.7895(10)$ Å, $c = 11.3454(8)$ Å, and $Z = 4$. $BaDyCuTe_3$ is isotypic with the known structure of $KZrCuS_3$. The other compounds, $K_{0.5}Ba_{0.5}DyCu_{1.5}Te_3$ and $K_{1.5}Dy_2Cu_{2.5}Te_5$, belong to new structure types. The structure of the former compound is a filled version of the $BaDyCuTe_3$ compound noted above. However, unlike $BaDyCuTe_3$, $K_{0.5}Ba_{0.5}DyCu_{1.5}Te_3$ crystallizes in the noncentrosymmetric orthorhombic space group $Cmc2_1$ (no. 36) with cell dimensions of $a = 4.3877(3)$ Å, $b = 14.9001(12)$ Å, $c = 11.4847(9)$ Å, and $Z = 4$. While $BaDyCuTe_3$ contains infinite one-dimensional chains of tetrahedra with stoichiometry $[CuTe_3^{5-}]_\infty$, the new phase $K_{0.5}Ba_{0.5}DyCu_{1.5}Te_3$ forms a three-dimesional framework of tetrahedra. The compound $K_{1.5}Dy_2Cu_{2.5}Te_5$ crystallizes in another orthorhombic space group, *Pmnn* (No. 58) with cell axes of $a = 4.3307(1)$ Å, $b = 16.6766(2)$ Å, $c = 17.6945(2)$ Å, and $Z = 4$. This final structure can also be related to that of $K_{0.5}Ba_{0.5}DyCu_{1.5}Te_3$.

Introduction

One theme in crystal chemistry as well as in materials chemistry has been tetrahedral coordination because it leads to compounds of both structural and technological importance.[1] Aside from the utility of aluminosilicate zeolites in catalytic applications, recent interest in photonic technology, especially in second-order nonlinear optical (NLO) devices, has initiated the search for noncentrosymmetric tetrahedral chalcogenides. These latter compounds may surpass the well-established oxide counterparts in their NLO properties.[2] To encourage the crystallization in acentric space groups (a prerequisite for second-order NLO materials), main group elements such as Ge have been used to form noncentrosymmetric tetrahedral coordination environments.[2] Acentric tetrahedra do not ensure the whole crystal structure to be acentric, yet the chance that a compound will crystallize with a noncentrosymmetric space group is greater than when centrosymmetric polyhedra are involved.[2,3] Indeed, the remarkable beauty and the diversity of the tetrahedral structures of silicates have fascinated many solid-state chemists for the past few decades.[4] The great variety of the tetrahedral structures found in natural or synthetic silicates ranges from simple tetrahedral monomers to more complex structural motifs such as dimers, trimers, chains, rings, sheets, nets, and other complicated framework structures.[4,5] Similar tetrahedral structural motifs can also be found in the polyanionic part of Zintl phases such as $SiAs_4^{8-}$ in Ba_4SiAs_4 (monomers), $Al_2Sb_6^{12-}$ in $Ba_6Al_2Sb_6$ (dimers), $Sn_2P_6^{12-}$ in Ba_3SnP_3 (ethane-like dimers), $Sn_3Se_8^{4-}$ in $K_4Sn_3Se_8$ (trimers), $Ge_4Se_{10}^{4-}$ in $Cs_2Ge_2Se_5{\cdot}2CH_3OH$ (adamantane-like cages), SiP_2^{2-} in K_2SiP_2 (edge-sharing chains), and $AlAs_3^{6-}$ in Ca_3AlAs_3 (vertex-sharing chains), as well as polyanionic parts of chalcogenides with d-block elements with d^5 or d^{10} configuration such as FeS_2^- in $CsFeS_2$ (edge-sharing chains), ZnS_2^{2-} in Na_2ZnS_2 (edge-sharing chains), and FeS^{3-} in Cs_3FeS_3 (dimers).[6] While new tetrahedral Zintl phases have been and continue to be synthesized with the aid of electron-counting rules known as Zintl

(1) For reviews in tetrahedral compounds, see (a) Parthé, E. In *Modern Perspectives in Inorganic Crystal Chemistry*; Parthé, E., Ed.; Kluwer Academic Publishers: Dordrecht, Holland, 1992; p 177. (b) Parthé, E.; Chabot, B. *Acta Crystallogr.* **1990**, *B46*, 7. (c) Parthé, E. *Cristallochimie des Strucctures Tétraédriques*; Gordon & Breach: New York; 1972.

(2) Good examples of tetrahedral compounds crystallized in acentric space groups are structures as simple as ZnS as well as more complex sulfides such as quarternary $CsSmGeS_4$ and quinary $LaCa_2GeS_4Cl_3$. See (a) $CsSmGeS_4$: Bucher, C. K.; Hwu, S.-H. *Inorg. Chem.* **1994**, *33*, 5831.(b) $LaCa_2GeS_4Cl_3$: Gitzendanner, R. L.; DiSalvo, F. J. *Inorg. Chem.* **1996**, *35*, 2623.

(3) (a) Vaughey, J. T.; Corbett, J. D. *J. Am. Chem. Soc.* **1996**, *118*, 12098. (b) Keller, S. W. *Angew. Chem., Int. Ed. Engl.* **1997**, *36*, 247.

(4) (a) Mejer, W. M.; Olson, D. H. *Atlas of Zeolite Structure Types*, 2nd ed.; Butterworth Publication: London; 1987. (b) Occelli, M. L.; Robson, H. E. *Synthesis of Microporous Materials; Molecular Sieves*; van Nostrand Reinhold: New York; 1992; Vol. 1.

(5) (a) Liebau, F.; In *Handbook of Geochemistry*; Springer-Verlag; New York; 1970; Vol II-2; p 14-A-1. (b) Hyde, B. G.; Andersson, S. *Inorganic Crystal Structures*; Wiley: New York; 1989.

S0897-4756(97)00700-X CCC: $15.00
Published on Web 04/29/1998

rules, the efforts to explore such transition metal Zintl compounds have been very scarce until recently.[7]

The purpose of the present study is twofold. One is to realize a noncentrosymmetric crystal structure based on acentric tetrahedral building units, and the other is to find novel tetrahedral structural motifs unknown in silicates and Zintl phases. Here we present the syntheses and crystal structures of the new quarternary and quinary copper tellurides, $BaDyCuTe_3$, $K_{1.5}Dy_2Cu_{2.5}Te_5$, and $K_{0.5}Ba_{0.5}DyCu_{1.5}Te_3$. Of these $BaDyCuTe_3$ is isotypic with a previously established structure[11a] while the other two phases belong to new structure types. The compound $K_{0.5}Ba_{0.5}DyCu_{1.5}Te_3$ crystallizes in *Cmc*21, a noncentrosymmetric space group. We find new tetrahedral structural motifs in $K_{1.5}Dy_2Cu_{2.5}Te_5$ and $K_{0.5}Ba_{0.5}DyCu_{1.5}Te_3$, both based on three-dimensional tetrahedral frameworks.

Experimental Section

General Procedures. All the reagents were obtained from Aldrich. Nominal purities of the reagents were Dy 99.9+%, Cu 99%, Te 99.99%, Ba 99+%, LiCl 99.9+ %, KCl 99.99%, and $BaCl_2$ 99.95%. The Ba rods were ground into powder in mineral oil under a N_2 atmosphere. The KCl/LiCl flux was prepared by mixing LiCl and KCl in a 45:55 mole ratio, melting the mixture under flame (nominal mp 300 °C), and drying this mixture for several minutes under 10^{-3} Torr vacuum. We placed (as described below) the stated amounts of reagents in vacuum-sealed quartz tubes. The heating and cooling profiles for all the samples were the same and are as follows. The reaction mixtures were heated to 850 °C at 1 °C/min, held at this temperature for 3 days, and then cooled to 400 °C at 3 °C/h, at which point they were annealed for one week. After one week, the furnace was turned off, and the samples were cooled to room temperature while still in the furnace. The quartz tubes were then broken and the product was washed first with water and then acetone to remove first the salt and then the water. We analyzed single crystals by an electron microprobe (Cameca MBX automated microprobe, wavelength-dispersive spectrometry (WDS) for quantitative stoichiometry and KEVEX EDS for nonstandardized measurements). Standards for WDS measurements were $KAlSi_3O_8$ (adularia) for K, $Ba_5(PO_4)_3Cl$ for Ba and Cl, $Dy_3Ga_5O_{12}$ for Dy, CuS for Cu, and elemental Te for Te. Atomic absorption measurements were taken on a Perkin-Elmer 1100B atomic absorption spectrometer.

$BaDyCuTe_3$ (1). We placed 0.1 mmol of Ba, 0.1 mmol of Dy, 0.2 mmol of Cu, and 0.4 mmol of Te along with 0.6 g of $BaCl_2$ flux in a vacuum-sealed quartz tube. After the reaction, we found a number of different components. While the major component was in the form of black needles, other minor components included brown needles, purple blocks, and gray blocks. We selected several crystals from each kind and performed microprobe analysis. The microprobe results of all black needles gave a nearly equivalent atomic stoichiometry of $Ba_{0.17(1)}Dy_{0.16(1)}Cu_{0.17(2)}Te_{0.49(2)}$. The compositions of other minor components were $Dy_{0.23(2)}Cu_{0.17(2)}Te_{0.60(3)}$ (brown needles),[9] $Dy_{0.40(2)}Te_{0.60(1)}$ (purple blocks), and element Te (gray blocks) where the numbers in parentheses are standard deviations. A Guinier powder pattern of the reaction mixture showed one major compound, which proved to be $BaDyCuTe_3$, along with a trace of Dy_2Te_3. No other compound was found in the powder pattern.

$K_{0.5}Ba_{0.5}DyCu_{1.5}Te_3$ (2). We placed 0.1 mmol of Ba, 0.1 mmol of Dy, 0.1 mmol of Cu, and 0.2 mmol of Te along with 1 g of a LiCl/KCl (45:55) flux in a vacuum-sealed quartz tube. After the reaction, we found that the major components were in the form of black needles and the minor in black platelets. Several crystals of each types were selected for microprobe analysis. The microprobe results for the needles and platelets were $K_{0.080(2)}Ba_{0.064(3)}Dy_{0.15(1)}Cu_{0.24(1)}Te_{0.47(2)}$, and $K_{0.19(2)}Dy_{0.18(4)}Te_{0.61(3)}$, respectively. Black needles were separated from the others under the microscope for atomic absorption (AA) Li analysis. Li content was found to be below the limit determination (<0.01 at. %). A Guinier powder pattern of the reaction mixture showed a major component which proved to be $K_{0.5}Ba_{0.5}DyCu_{1.5}Te_3$. Only single crystals of the former compound were of sufficient quality for the recording of an X-ray data set. Long-exposure Weissenberg photographs (72 h) and long-exposure oscillation photographs (48 h) did not show any superstructure reflections.

$K_{1.5}Dy_2Cu_{2.5}Te_5$ (3). We placed 0.1 mmol of Dy, 0.1 mmol of Cu, and 0.2 mmol of Te along with 1 g of LiCl/KCl (45:55) flux in a vacuum-sealed quartz tube. After the reaction, the product primarily had the form of black needles. However, we did find a few gray platelets and purple grains. We selected several crystals of each form and performed microprobe analysis. The respective compositions for needles, platelets and grains were $K_{0.13(2)}Dy_{0.18(1)}Cu_{0.21(2)}Te_{0.46(1)}$, $K_{0.24(1)}Dy_{0.24(1)}Te_{0.51(2)}$, and $Cu_{0.62(2)}Te_{0.38(2)}$. AA Li analysis on the black needles, separated under the microscope, showed the content of Li was 0.03 at. %. A Guinier powder pattern showed a new compound, which turned out to be $K_{1.5}Dy_2Cu_{2.5}Te_5$, as well as two minor phases, Cu_3Te_2 and a new phase isostructural with $KErTe_2$. Cell dimensions for the last phase were refined with hexagonal symmetry with $a = 4.453(3)$ Å and $c = 24.419(4)$ Å. Due to the close similarity between this latter phase's powder pattern and that of $KErTe_2$ as well as the presence of platelets with a microprobe composition of $K_{0.24(1)}Dy_{0.24(1)}Te_{0.51(2)}$, we concluded that we had produced a phase $KDyTe_2$ which is isostuctural with $KErTe_2$.

Crystallographic Studies

All the samples were examined by the Guinier X-ray powder diffraction method (Enraf-Nonius Guinier camera, Cu Kα1 radiation, and NIST Si internal standard) for identification of reaction products. The theoretical intensities were generated by the Cerius[2] program[10a] and compared with the Guinier X-ray powder pattern obtained. Weissenberg (Cu Kα radiation) photographs were also taken to check the quality of crystals suitable for single-crystal X-ray data set collection. Long-

(6) (a) For reviews in Zintl phases, see Schafer, H.; Eisenmann, B. *Rev. Inorg. Chem.* **1981**, *3*, 101. Kauzlarich, S. M., Ed. *Chemistry, Structure, Bonding of Zintl Phases and Ions*; VCH: New York; 1996. (b) Ba_4SiAs_4: Eisenmann, B.; Jordan, H.; Schaefer, H. *Angew. Chem.* **1981**, *93*, 211, (c) Ba_3AlSb_3 and Ca_3AlAs_3: Cordier, G.; Salvelsberg, G.; Schaefer, H. *Z. Naturforsch.* **1982**, *B37*, 975. (d) Ba_3SnP_3: Eisenmann, B.; Jordan, H.; Schaefer, H. *Z. Naturforsch.* **1983**, *B38*, 404. (e) $K_4Sn_3Se_8$: Sheldrick, W. *Z. Naturforsch.* **1988**, *B43*, 249. (f) $Cs_2Ge_2Se_5{\cdot}CH_3OH$: Sheldrick, W. S.; Schaaf, B. *Z. Naturforsch.* **1995**, *B49*, 655. (g) K_2SiP_2: Eisenmann, B.; Somer, M. *Z. Naturforsch.* **1984**, *B39*, 736. (h) $CsFeS_2$: Bronger, W. *Z. Anorg. Allg. Chem.* **1968**, *359*, 225. (i) Na_2ZnS_2: Klepp, K. O.; Bronger, W. *Rev. Chim. Miner.* **1983**, *20*, 682. (j) Cs_3FeS_3: Bronger, W.; Ruschewitz, U.; Mueller, P. J. *Less-Common Met.* **1992**, *187*, 95.

(7) (a) Dhingra, S. S.; Haushalter, R. C. *J. Am. Chem. Soc.* **1994**, *116*, 3651. (b) Young, D. M.; Charlton, J.; Olmstead, M. M.; Kauzlarich, S. M.; Lee, Chi-Shen; Miller, G. J. *Inorg. Chem.* **1997**, *36*, 2539. (c) Kauzlarich, S. M. In *Chemistry, Structure, Bonding of Zintl Phases and Ions*; Kauzlarich, S. M., Ed.; VCH: New York; 1996.

(8) (a) BaCdSnS4: Teske, C. L. *Z. Anorg. Allg. Chem.* **1980**, *460*, 163.

(9) Huang, F. Q.; Lee, S. Unpublished data.

(10) (a) The Cerius[2] program is commercially available from Molecular Simulations, Waltham, MA 02154. (b) Refinements were carried out with the Shelxl-93 package with refinement against F^2 vs F. For comparative purposes to traditional refinement we report the standard R-factor (for reflections where $I > 2s(I)$ as well as wR_2. See Sheldrick, G. M. *Acta Crystallogr.* **1990**, *A46*, 467.

(11) (a) $KZrCuS_3$: Mansuetto, M. F.; Keane, P. M.; Ibers, J. A. *J. Solid State Chem.* **1992**, *101*, 257. Recent additions to this structure type include (b) $BaErCuS_3$, $BaYAgSe_3$: Wu, P.; Christuk, A. E.; Ibers, J. A. *J. Solid State Chem.* **1994**, *110*, 337. (c) $CsCuCeS_3$, $KCuUSe_3$: Sutorik, A. C.; Albritton-Thomas, J.; Hogan, T.; Kannewurrff, C. R.; Kanatzidis; M. G. *Chem. Mater.* **1996**, *8*, 751. (d) $CsCuUTe_3$: Cody, J. A.; Ibers, J. A. *Inorg. Chem.* **1995**, *34*, 3165.

Table 1. Selected Crystallographic Data for $BaCuDyTe_3$, $K_{0.5}Ba_{0.5}DyCu_{1.5}Te_3$, and $K_{1.5}Dy_2Cu_{2.5}Te_5$

empirical formula	$BaCuDyTe_3$	$K_{0.5}Ba_{0.5}DyCu_{1.5}Te_3$	$K_{1.5}Dy_2Cu_{2.5}Te_5$
crystal color, habit	black, needle	black, needle	black, needle
crystal size	0.12 × 0.02 × 0.02	0.72 × 0.10 × 0.06	0.40 × 0.02 × 0.02
crystal system	orthorhombic	orthorhombic	orthorhombic
space group	*Cmcm* (no. 63)	$Cmc2_1$ (no. 36)	*Pmnn* (no. 58)
Z	4	4	4
a (Å)	4.4286(3)	4.3877(3)	4.3307(1)
b (Å)	14.7895(10)	14.9001(12)	16.6766(2)
c (Å)	11.3454 (8)	11.4847(9)	17.6945(2)
volume (Å^3)	743.08(15)	750.84(17)	1277.918(36)
density (calc) (g cm^{-3})	6.670	6.447	6.136
linear abs coeff μ (cm^{-1})	294.5	282.4	272.7
no. data collected	3835	2421	12680
no. unique reflns	563	986	1853
obsd reflns ($I \geq 2\sigma(I)$)	496	982	1618
N parameters refined	24	43	77
data/parameter ratio	23.5	22.9	22.3
R/wR_2 (obs data)	0.0373/0.0717	0.0394/0.0920	0.0263/0.0383
R/wR_2 (all data)	0.0434/0.0729	0.0395/0.0921	0.0346/0.0395
goodness of fit (obs data)	1.792	1.577	1.312
goodness of fit (all data)	1.707	1.575	1.263
mean shift/error	0.000	0.000	−0.001
maximum shift/error	0.000	0.000	0.000
secondary extinction (x)[a]	0.0016(2)	0.0022(2)	0.00112(4)
weighting scheme	$w^{-1} = [\sigma^2(F_o) + (0.02P)^2 + 0.00P]$ where $P = (\max(F_o^2, 0) + 2F_c^2)/3$	$w^{-1} = [\sigma^2(F_o) + (0.04P)^2 + 0.00P]$	$w^{-1} = [\sigma^2(F_o) + (0.00P)^2 + 0.00P]$
residual electron density	2.476 and −2.487 e$^-$/Å^3	3.059 and −2.677 e$^-$/Å^3	1.459 and −1.507 e$^-$/Å^3

[a] An extinction parameter x is defined by least-squares using the formula $F_c = kF_c[1 + 0.01F_c^2\,\lambda^3/\sin(2\theta)]^{-1/4}$ where k is the overall scale factor.

exposure Weissenberg photographs and ocsillation photographs were taken for $K_{0.5}Ba_{0.5}DyCu_{1.5}Te_3$ to check for superstructure reflections. A summary of the selected crystallographic data is listed in Table 1 and the conditions for the data sets appear in the Supporting Information. The structure solutions were obtained by direct method using SHELXS-86 and were refined using full-matrix analysis on all reflections, based on F_o^2, with SHELXL-93.[10b]

Structure Determination of $BaDyCuTe_3$. A crystal with dimensions of 0.12 × 0.02 × 0.02 mm^3 was chosen for the data set collection. The space groups corresponding to the observed systematic extinction conditions are the orthorhombic space groups *Cmcm*, $Cmc2_1$, and *C*2*cm*. We refined the structure in the centrosymmetric group *Cmcm*, the highest symmetry space group of the three. Initial atomic coordinates obtained from the direct method compared well with those from the known crystal structure of $KZrCuS_3$ (which is known to be in space group *Cmcm*) and led to an isotropic refinement with $R = 5.32\%$ and $wR_2 = 8.68\%$ for 12 parameters and 563 reflections.[10b] The stoichiometry at this point corresponded to $BaDyCuTe_3$. We then switched to anisotropic refinement. This yielded $R = 4.34\%$ and $wR_2 = 7.29\%$ with 24 parameters. The highest peak in the Fourier difference map is located near Te1 at a distance of 0.78 Å. The height of this peak is 2.476 e$^-$/Å^3. The final refinement stoichiometry is $BaDyCuTe_3$ in good agreement with both the microprobe analysis data $Ba_{1.0(1)}Dy_{0.94(6)}Cu_{1.0(1)}Te_{2.9(1)}$ and the charge balance condition assuming the canonical oxidation states $Ba^{2+}Dy^{3+}Cu^{1+}(Te^{2-})_3$. Lowering the symmetry to acentric $Cmc2_1$ or *C*2*cm* led to no meaningful decrease in the *R* factor. Final atomic coordinates, occupation factors, and isotropic thermal factors are given in Table 2, and bond distances are given in Table 3. The relative intensities of the calculated powder pattern based on this single-crystal data agree well with those obtained experimentally. Anisotropic thermal parameters for $BaDyCuTe_3$ appear in the Supporting Information.

Table 2. Atomic Positions for $BaDyCuTe_3$

atom	*x*	*y*	*z*	occupancy	U_{eq}
Ba1	0.0000	0.24982(8)	0.7500	1.0	0.0166(3)
Dy1	0.0000	0.5000	0.5000	1.0	0.0124(2)
Cu1	0.5000	0.5331(2)	0.2500	1.0	0.0224(5)
Te1	0.0000	0.42931(8)	0.2500	1.0	0.0122(3)
Te2	0.5000	0.63767(6)	0.44060(6)	1.0	0.0126(2)

Table 3. Interatomic Distances (Å) for $BaDyCuTe_3$

Ba1	2Te1	3.4528(13)
	4Te2	3.5140(8)
	2Te2	3.8825(9)
Dy1	2Te1	3.0229(4)
	4Te2	3.0826(6)
Cu1	2Te1	2.695(2)
	2Te2	2.658(2)

Structure Determination of $K_{0.5}Ba_{0.5}DyCu_{1.5}Te_3$. A crystal with dimensions of 0.72 × 0.10 × 0.06 mm^3 was chosen for the data set collection. The space groups corresponding to the systematic extinction conditions are *Cmcm*, $Cmc2_1$, and *C*2*cm*. We initially refined the structure in the space group *Cmcm*, the highest space group of the three. An isotropic refinement based on direct method solution led to a structure nearly equivalent to the one found for $BaDyCuTe_3$ except that in addition to all the atomic sites of the $BaDyCuTe_3$ structure there is an additional copper site, Cu2, which is 25% filled. The *R*- and wR_2-values were rather high, being 22.71% and 54.26%, respectively, for 15 parameters and 540 reflections. As this is a rather high *R*-factor for an isotropic refinement, we therefore examined the two noncentrosymmetric space groups $Cmc2_1$ and *C*2*cm*. Both $Cmc2_1$ and *C*2*cm* are subgroups of *Cmcm*. The original 8f position of *Cmcm* decomposes in $Cmc2_1$ to two symmetry-unrelated 4a positions while in *C*2*cm* it transforms into a general 8a position. In our original *Cmcm* refinement there are two atomic sites with 8f multiplicity and Wyckoff letter, the Te2 and Cu2

position. Furthermore the 8f site for Cu2 is only 25% filled in *Cmcm*. In passing to the noncentrosymmetric groups, $Cmc2_1$, we find that one of the two corresponding Cu4a positions is a quarter occupied while the other is completely empty. The isotropic *R*-factor for $Cmc2_1$ and *C*2*cm* are, respectively, $R = 7.14\%$ $wR_2 = 21.75\%$ for 23 parameters and 986 reflections and $R = 19.89\%$ and $wR_2 = 57.51\%$ for 21 parameters and 896 reflections. Clearly in the former case the drop in *R*-factors is statistically significant. It is interesting to note that this large drop in *R*-factors occurs even though the copper atoms are the lightest atoms in the structure refinement. In fact this disproportionation of the copper site in going from *Cmcm* to $Cmc2_1$ primarily lowers the *R*-factors not by its direct effect on the Cu2 site but rather by its indirect effect on the Te2 site. As noted above, this Te2 site is also in an 8f position in *Cmcm* which converts into two symmetrically inequivalent 4a positions in $Cmc2_1$. These are the Te2 and Te3 sites of the final refined structure. Both the Te2 and Te3 sites are bonded to Cu2, but each Te2 is bonded to two different Cu2 atoms while each Te3 atom is bonded to only one Cu2 atom. As a consequence, in $Cmc2_1$, the Te2 and Te3 positions are only partially related by inversion symmetry. This loss of true inversion symmetry for these tellurium atoms is one of the principal causes of the change in *R*-factors in passing from *Cmcm* to $Cmc2_1$. In fact, the single additional parameter corresponding to the loss of an inversion center relation between the *b*-axis components of Te2 and Te3 accounts by itself for a drop in *R*-factor of roughly 0.06.

There are two additional interesting points in our refinement of this structure. We noticed that the thermal factor for the Ba site (M1) is larger than that of most of the other sites (e.g. $U_{iso} = 0.06$ vs $U_{iso} \sim 0.02$ for other elements) Therefore we allowed K atoms to occupy this site and refined the occupation factors of these two elements, fixing the sum of the K and Ba occupation factors to correspond to full occupancy and keeping the thermal factors for these two atoms the same. The resulting occupation factors were, respectively, 45.12% and 54.88% for K and Ba with $R = 6.13\%$ and $wR_2 = 16.48\%$, a 0.013 drop in the overall *R*-factor. We found that one of the copper sites (Cu2) also had a larger thermal factor compared with the other copper site (e.g. $U_{iso} = 0.065$ vs $U_{iso} \sim 0.03$). Hence we allowed the occupation of this site to be refined while constraining the isotropic thermal factors for the two copper sites to be equal. The Cu2 site refined to a copper occupation factor of 54.62%. The overall refinement had a significantly lower $R = 5.13\%$ and $wR_2 = 13.67\%$ for 24 parameters. The refined stoichiometry at this stage was $K_{0.54}Ba_{0.45}Dy_1Cu_{1.55}Te_3$. At this point we switched to anisotropic refinement. The *R* and *wR*2 then became 4.21% and 10.65%, respectively, for 42 parameters. Finally, because the space group is a noncentrosymmetric one we tested for the possiblity of racemic twinning. The refinement after including one additional parameter for racemic twinning led to $R = 3.95$ and $wR_2 = 9.21$ for 43 parameters and 986 reflections. This final drop in *R*-factors is significant according to Hamilton's test. As a final test of our refinement we released simultaneously the occupation factors on all metal positions, keeping tellurium occupation factors fixed.

Table 4. Atomic Positions for $K_{0.5}Ba_{0.5}DyCu_{1.5}Te_3$

atom	*x*	*y*	*z*	occupancy	U_{eq}
M1	0.0000	0.75166(13)	−0.7426(2)	1.0	0.0334(6)
Dy1	0.0000	0.48863(5)	0.49560(6)	1.0	0.0217(2)
Cu1	0.5000	0.4659(2)	0.7430(3)	1.0	0.0311(4)
Cu2	0.0000	0.6813(3)	0.5482(4)	0.575(8)	0.0311(4)
Te1	0.0000	0.43108(7)	−0.75950(9)	1.0	0.0193(2)
Te2	0.0000	0.12934(7)	−0.56165(9)	1.0	0.0204(3)
Te3	0.0000	0.85527(7)	0.56019(8)	1.0	0.0191(3)

[a] M1 is 45% Ba and 55% K.

Table 5. Interatomic Distances (Å) for $K_{0.5}Ba_{0.5}DyCu_{1.5}Te_3$

M1	2Te1	3.464(2)
	2Te2	3.529(2)
	2Te3	3.533(2)
	1Te3	3.805(3)
Dy1	1Te1	3.0527(12)
	1Te1	3.0564(12)
	2Te2	3.1049(9)
	2Te3	3.0517(8)
Cu1	2Te1	2.6773(13)
	1Te2	2.655(3)
	1Te3	2.670(3)
Cu2	1Te1	2.772(5)
	2Te2	2.647(2)
	1Te3	2.595(4)

Neither *R*-factors nor metal occupation factors changed appreciably, the metal occupation factors not changing by more than 3% from their original values. The final stoichiometry is $K_{0.56}Ba_{0.44}Dy_{1.00}Cu_{1.54}Te_3$, in good agreement with both microprobe analysis ($K_{0.53(2)}Ba_{0.43(2)}Dy_{1.0(1)}Cu_{1.6(1)}Te_{3.1(1)}$) and with the assignment of oxidation states of +1, +2, +3, +1, and −2 for, respectively, the potassium, barium, dysprosium, copper, and tellurium atoms ($0.56+2 \times 0.44+3 \times 1.00+1.54 = 5.98 \approx 2 \times 3.00$). Final atomic coordinates, occupation factors, and isotropic thermal factors are given in Table 4 and bond distances in Table 5. The relative intensities of the calculated powder pattern based on this single-crystal data agree well with those obtained experimentally. Anisotropic thermal parameters for this compound appear in the Supporting Information.

Structure Determination of $K_{1.5}Dy_2Cu_{2.5}Te_5$. A crystal with dimensions of $0.40 \times 0.02 \times 0.02$ mm^3 was chosen for the data set collection. The space groups corresponding to the observed systematic extinction conditions are *Pmnn* and *P*2*nn*. We refined the structure in *Pmnn*, the higher symmetry group of the two. An initial solution based on direct method led to an isotropic refinement where $R = 6.30\%$ and $wR_2 = 13.24\%$ for 37 parameters and 1853 reflections. We located three copper sites in this refinement. However, one of the copper sites had an unusally large thermal factor compared to that of the other two copper sites ($U_{iso} = 0.16$ vs $U_{iso} \sim 0.023$ for other Cu sites). We therefore allowed the occupation of this site to be refined. The Cu3 site refined to a Cu occupation factor of 40% with $R = 5.02\%$ and $wR_2 = 9.18\%$ for 38 parameters. The composition at this point was $K_{1.5}Dy_2Cu_{2.4}Te_5$. At this point we noticed that the highest peak in the Fourier difference map was located in a tetrahedral site surrounded by four Te atoms (Te1 and Te3) of sufficient dimension to fit an additional copper atom. We included this site (Cu4) in the refinement. The resulting occupation factors for both Cu3 and Cu4 occupation factors were, respectively, 40.5% and 8.9%

Table 6. Atomic Positions for $K_{1.5}Dy_2Cu_{2.5}Te_5$

atom	*x*	*y*	*z*	occupancy	U_{eq}
K1	0.5000	0.5000	0.0000	1.0	0.0389(7)
K2	0.0000	0.82943(11)	0.66461(11)	1.0	0.0262(4)
Cu1	0.5000	0.84184(7)	0.34663(6)	1.0	0.0251(2)
Cu2	0.5000	0.43637(6)	0.45948(5)	1.0	0.0224(2)
Cu3	0.0000	0.5929(2)	0.31085(14)	0.408(6)	0.0266(9)
Cu4	0.0000	0.5239(8)	0.4529(7)	0.086(5)	0.031(5)
Dy1	0.0000	0.71236(2)	0.44700(2)	1.0	0.01364(9)
Dy2	0.5000	0.43434(2)	0.28435(2)	1.0	0.01374(9)
Te1	0.5000	0.58595(3)	0.39381(3)	1.0	0.01274(11)
Te2	0.0000	0.77079(3)	0.28623(3)	1.0	0.01488(11)
Te3	0.0000	0.62994(3)	0.60240(3)	1.0	0.01272(11)
Te4	0.5000	0.82749(3)	0.49602(3)	1.0	0.01454(11)
Te5	0.0000	0.50205(3)	0.18403(3)	1.0	0.01551(11)

Table 7. Interatomic Distances (Å) for $K_{1.5}Dy_2Cu_{2.5}Te_5$

K1	4Te4	3.6013(5)
	4Te5	3.9109(5)
K2	2Te2	3.481(2)
	1Te3	3.502(2)
	2Te4	3.685(2)
	2Te5	3.566(2)
Cu1	2Te2	2.6898(7)
	1Te4	2.6542(11)
	1Te5	2.7263(12)
Cu2	1Te1	2.7518(12)
	1Te1	2.6225(11)
	2Te3	2.6665(6)
	1Cu2	2.561(2)
Cu3	2Te1	2.6186(15)
	1Te2	2.998(3)
	1Te5	2.708(3)
Dy1	2Te1	3.1652(4)
	1Te2	3.0070(6)
	1Te3	3.0741(6)
	2Te4	3.0212(4)
Dy2	1Te1	3.1848(6)
	1Te2	2.9997(6)
	2Te3	3.1390(4)
	2Te5	3.0191(4)

with $R = 4.79\%$ and $wR_2 = 8.68\%$ for 41 parameters while the Cu1 and Cu2 sites had full occupation. At this stage we applied an anisotropic refinement on all sites except for Cu4, whose low occupation factor did not warrant anisotropic refinement. This refinement resulted in $R = 3.46\%$ and $wR_2 = 3.95\%$ for 77 parameters. As a final test for our structural model we released simultaneously the occupation factors for all the metal atom positions except Cu4 while keeping the tellurium occupation factors fixed. *R*-factors did not change appreciably, and metal occupation factors did not change by more than 1% from their original values. The final stoichiometry is $K_{1.5}Dy_2Cu_{2.48}Te_5$, in good agreement with both microprobe analysis ($K_{1.4(2)}Dy_{2.0(1)}Cu_{2.3(2)}Te_{5.0(2)}$) and with the assignment of oxidation state of +1, +2, +3, +1, and −2 for, respectively, potassium, barium, dysprosium, copper, and tellurium atoms ($1.5+3 \times 2+2.48 = 9.98 \approx 2 \times 5$). Final atomic coordinates, occupation factors, and isotropic thermal factors are given in Table 6 and bond distances in Table 7. The relative intensities of the calculated powder pattern based on these single-crystal data agree well with the ones obtained experimentally. Anisotropic thermal parameters for $K_{1.5}Dy_2Cu_{2.5}Te_5$ appear in the Supporting Information.

Discussion

The compound $BaDyCuTe_3$ (**1**) is isostructural to $KZrCuS_3$.[11] Atomic coordinates and bond distances are shown in Tables 2 and 3, respectively. In Figure 1a we illustrate the structure of **1**. In Figure 1a, as in all the

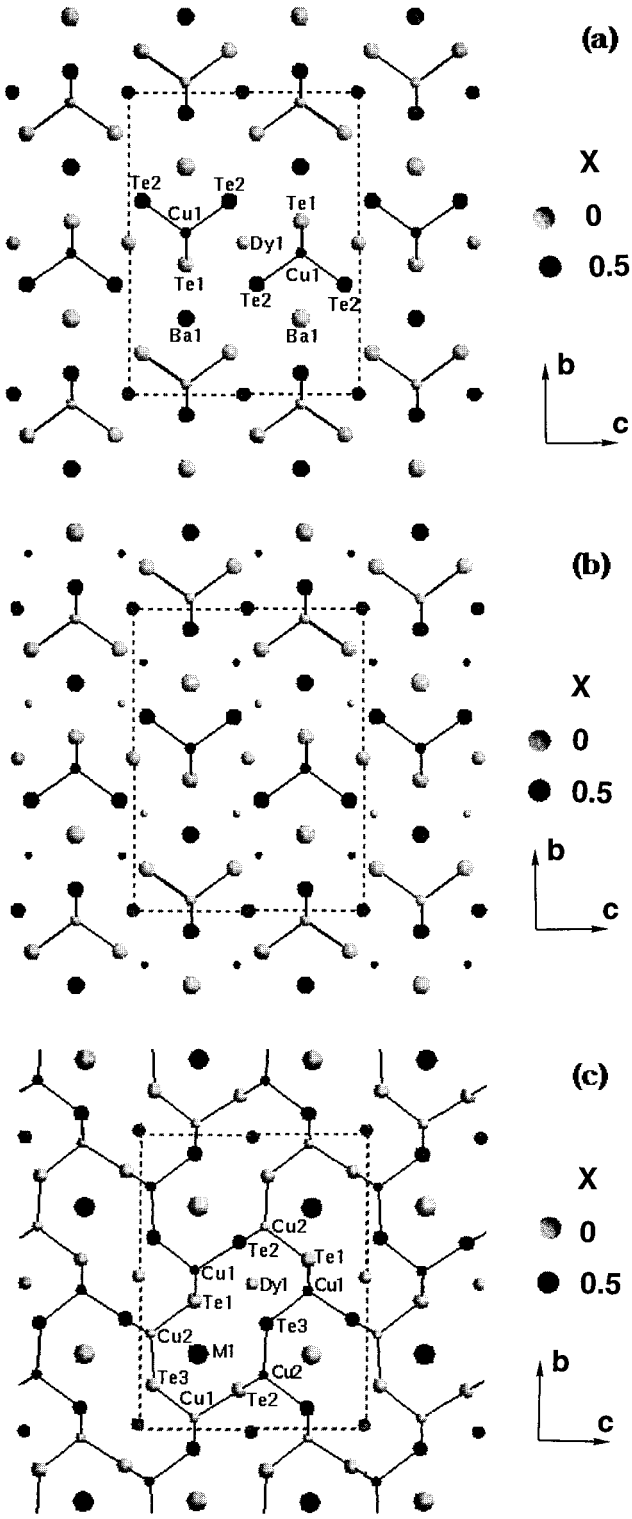

Figure 1. The [100] projections of the structures of $BaDyCuTe_3$ and $K_{0.5}Ba_{0.5}DyCu_{1.5}Te_3$. (a) The $BaDyCuTe_3$ structure viewed down the [100] axis. Open and closed circles correspond to atoms at, respectively, $x = 0$ and $x = 0.5$. Only the copper−tellurium bonds are drawn in the figures. (b) The empty tetrahedral site found in the $BaDyCuTe_3$ structure with empty tetrahedral sites viewed down the [100] axis. These empty tetrahedral sites are represented by the smallest circles. In this figure, as in the preceding diagram, open circles and closed circles correspond to atoms at, respectively, $x = 0$ and $x = 0.5$. (c) The $K_{0.5}Ba_{0.5}DyCu_{1.5}Te_3$ structure viewed down the [100] axis.

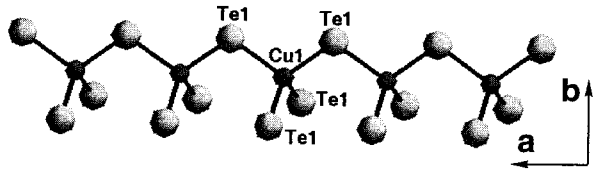

Figure 2. An Einer-einfachketten (single simple chain) $[CuTe_3^{5-}]_\infty$ of $BaDyCuTe_3$ running along [100] direction.

illustrations in this paper, we show only the copper to tellurium bonds and none of the bonds between dysprosium and tellurium. In this manner one can clearly see the $CuTe_4$ tetrahedral structural motif. As Figure 1a shows, there are one-dimensional tetrahedral chains $[CuTe_3^{5-}]_\infty$ running along the [100] direction as illustrated in Figure 2. This chain is based on vertex-sharing tetrahedra in "Einer-einfachketten" fashion (single simple chains) using Liebau's nomenclature.[13] The same one-dimensional chain structural motif can be found in Zintl phases such as Ca_3AlAs_3, Eu_2CuS_3, and $LaPbCuS_3$.[12] In transition metal Zintl compounds, however, such vertex-sharing tetrahedral chains are not common. More common in transition metal chalcogenides are edge-sharing chains as are found in structures such as $AFeS_2$ (A = K, Rb, and Cs), $CsGa_{0.75}Fe_{0.25}S_2$, $K_2HgSnTe_4$, and Na_2ZnS_2.[14] In compound **1**, these more unusual Einer-einfachketten are separated from one another by both dysprosium and barium atoms. Dysprosium atoms occupy octahedral sites while Ba atoms reside in larger bicapped trigonal prismatic sites.

Figure 1c shows the crystal structure of $K_{0.5}Ba_{0.5}DyCu_{1.5}Te_3$ (**2**). This structure belongs to a new structure type. Atomic coordinates and bond distances are shown in Tables 4 and 5, respectively. This structure is a filled version of the previous structure **1** and can be derived from **1**.[15] It is interesting to note that both cell dimensions and the atomic sites between two structures **1** and **2** are essentially equivalent except for the Cu2-filled tetrahedral sites in the structure **2**. These tetrahedral sites differentiate these two structures **1** and **2** from each other. In Figure 1b we include eight empty tetrahedral sites per unit cell which may be found in the crystal structure of $BaDyCuTe_3$. The partial replacement of Ba atoms by K atoms in going from $BaDyCuTe_3$ to $K_{0.5}Ba_{0.5}DyCu_{1.5}Te_3$ together with the requirement of charge neutrality necessitates the addition of two copper atoms per unit cell to replace the loss of the two valence electrons in potassium as opposed to barium (recall $Z = 4$). Among the possible eight empty tetrahedral sites of $BaDyCuTe_3$ four of these sites

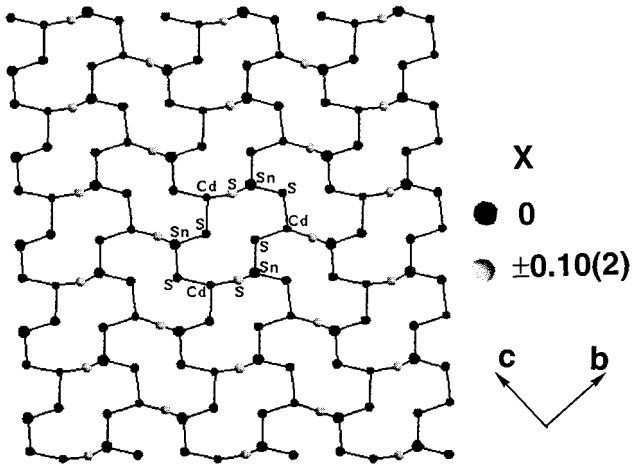

Figure 3. The [100] projection of a single two-dimensional net found in $BaCdSnS_4$. Closed and open circles are, respectively, at $x = 0$ and $x = \pm 0.10(2)$. Ba atoms are omitted to clearly illustrate the 12-membered rings formed by SnS_4 and CdS_4 tetrahedral units.

are half-occupied in the $K_{0.5}Ba_{0.5}DyCu_{1.5}Te_3$ structure while the remaining other four sites are completely unoccupied. It is this occupation of four tetrahedral sites and nonoccupation of the other four sites that is responsible for the loss of inversion center symmetry in going from $BaDyCuTe_3$ to $K_{0.5}Ba_{0.5}DyCu_{1.5}Te_3$. Like the original copper atoms in $BaDyCuTe_3$, the new copper atoms themselves form one-dimensional tetrahedral chains. However, these chains are now interconnected to adjacent one-dimensional copper chains, and therefore the overall structure is a three-dimensional one.

Another interesting structural point is that the Dy atoms as well as disordered K and Ba atoms reside inside rings formed by these interlocking copper−telluride tetrahedral chains. In Figure 1c these cavities have the form of 12-membered rings of alternating copper and tellurium atoms. Of interest is that this same pattern can be seen in the structure of $BaCdSnS_4$ as is shown in Figure 3.[8] It would be a mistake, however, to conclude that $BaCdSnS_4$ and $K_{0.5}Ba_{0.5}DyCu_{1.5}Te_3$ are isostructural. The difference between these two structures can be seen if one notes that the light and dark colored spheres in Figure 1 correspond to atoms at respective heights of zero and one-half. By contrast, in Figure 3 they correspond respectively to single atoms at height zero and pairs of atoms at height $+x$ and $-x$. Thus in Figure 3 while the overall structure is indeed made up of cadmium−tin−sulfur tetrahedra, these tetrahedra are edge-sharing rather than vertex-sharing. The resultant structure is a two-dimensional net instead of a three-dimensional one.

The final structure $K_{1.5}Dy_2Cu_{2.5}Te_5$ (**3**) is illustrated in Figure 4. This structure also belongs to a new structure type. Atomic coordinates and bond distances are shown in Tables 6 and 7, respectively. This structure contains similar structural fragments found in **2**. In particular we have again infinite chains of vertex-sharing $[CuTe_3^{5-}]_\infty$ chains running along the x-axis which interlock together to form a three-dimensional network. There are two principal differences between this and the preceding structure. First, in the latter structure the potassium and dysprosium atoms lie in 24-member rings of alternating copper and tellurium

(12) (a) Ca_3AlAs_3: see ref 6c (a) Eu_2CuS_3: Lemoine, P.; Carr, D.; Guittard, M. *Acta Crystallogr.* **1986**, *C42*, 390. (b) $LaPbCuS_3$: Brennan, T. D.; Ibers, J. A. *J. Solid State Chem.* **1992**, *97*, 377.

(13) Liebau classified many tetrahedral chain patterns found in silicates.[5a] In oxides, such a chain is rare and examples can be found in $CuGeO_3$ and $K_4Cu_2P_8O_{24}$. See (a) $CuGeO_3$: Völlenkle, H.; Wittmann, A.; Nowotny, H. *Monatsh. Chem.* **1967**, *98*, 1352. (b) $K_4Cu_2P_8O_{24}$: Tordjman, I.; Tran Qui, D.; Laügt, M. *Bull. Soc. Franç. Mineral. Crist.* **1970**, *93*, 160.

(14) (a) $KFeS_2$: Bronger, W.; Kyas, A.; Muller, P. *J. Solid State Chem.* **1987**, *70*, 262. (b) $RbFeS_2$: Bronger, W. *Z. Allog. Allg. Chem.* **1968**, *359*, 225. (c) $CsFeS_2$: ref 6f (d) $CsGa_{0.75}Fe_{0.25}S_2$: Bronger, W. Muller, P. *J. Less-Common Met.* **1980**, *70*, 253. (e) $K_2HgSnTe_4$: Dhingrass, S. S.; Haushalter, R. C. *Chem. Mater.* **1994**, *6*, 2376 (f) Na_2ZnS_2: ref 6g.

(15) It is interesting to note that the previous structure **1** itself is also a filled version of $FeUS_3$. See (a) ref 11a and (b) $FeUS_3$: Noël, H.; Padiou, J. *Acta Crystallogr.* **1976**, *B32*, 1593.

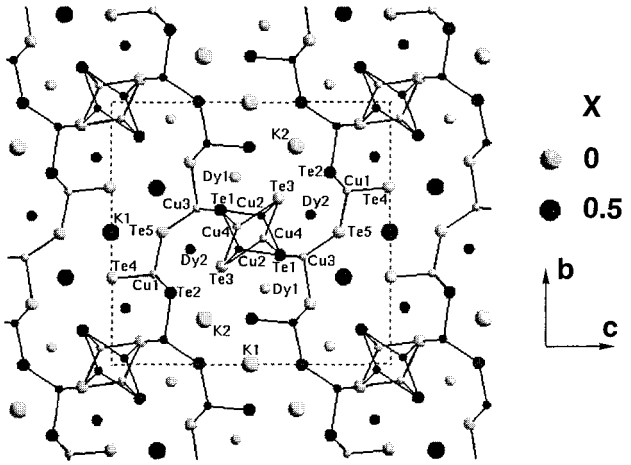

Figure 4. The $K_{1.5}Dy_2Cu_{2.5}Te_5$ structure viewed down the [100] axis. Open and closed circles correspond to atoms at, respectively, $x = 0$ and $x = 0.5$. We show only the copper to tellurium bonds to clearly indicate the $CuTe_4$ tetrahedral structural motif.

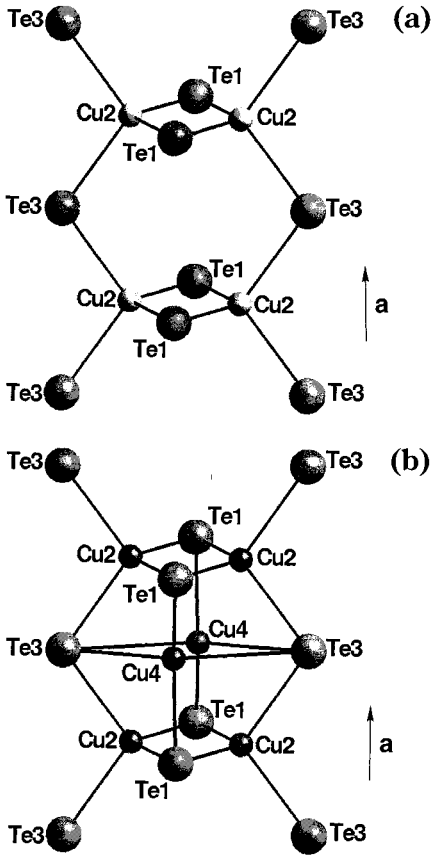

Figure 5. Polyhedral fragment found in $K_{1.5}Dy_2Cu_{2.5}Te_5$ (a) without the Cu4 site included (b) with the Cu4 site included.

atoms. The previous 12-member rings have therefore fused together to generate the new 24-member rings. Second, a new type of chain running in the [100] direction can be identified. This is illustrated in Figure 5a. The fundamental unit in this chain is two fused Einer-einfachketten; therefore the overall chain structure is an Einer-Doppelkette(double chain). There is an additional feature to the Einer-Doppelkette. In this chain structure there are vacant tetrahedral sites along the chain. In our case copper atoms reside in such sites (Cu4 site in Figure 5b). However, it should be recalled that the occupation of the Cu4 site is roughly only 10%. Each tetrahedral Cu4 site is edge-sharing with four adjacent Cu2 sites (see Figure 5b).

Another interesting point worth mentioning here is the Cu2−Cu2 distance (2.62 Å) observed between two edge-sharing tetrahedra in Figure 5a. This can be compared to the Cu−Cu bond distance of 2.56 Å observed in elemental Cu. At first glance it is rather surprising to find such a short distance because in our case copper is nominally in a d^{10} state. There are other however numerous reported examples of such short copper−copper distance. For example, the three compounds KCu_3Te_2, $NaCu_3Te_2$, and $C_{58}H_{46}Cu_2N_6S_4{\cdot}2(CH_3NO_2)$ have Cu−Cu distances of respectively 2.50−2.70, 2.51, and 2.63 Å.[16] The literature of $d^{10}-d^{10}$ bonds has recently been reviewed.[17] At a computational level, net attractive Cu(I)−Cu(I) interactions require the introduction of configuration interaction to the Hartree−Fock solutions. It is useful to note that in our case as well as in the compounds KCu_3Te_2, $NaCu_3Te_2$, and $C_{58}H_{46}Cu_2N_6S_4{\cdot}2(CH_3NO_2)$ that the short Cu−Cu distances are found between two edge-sharing copper telluride tetrahedra. We may therefore examine the central Cu2−Te1−Cu2−Te1 (see Figure 5a) square formed by the two edge-sharing tetrahedra to see if there are any distortions which indicate the presence of a Cu−Cu interaction. There are two kinds of bond angles in this central square, a Te1−Cu2−Te1 angle of 123.33(9)° and a Cu2−Te1−Cu2 bond angle of 56.67(9)°. The fact that the Te−Cu−Te angle has opened up from the ideal tetrahedral angle of 109.5° provides evidence for incipient copper−copper interaction.

Acknowledgment. The authors are grateful for the assistance of Carl Henderson of the University of Michigan Electron Microbeam Analysis Laboratory for microprobe analysis, Dr. Jeff Kampf of the University of Michigan Chemistry Department as well as Dr. Scott Wilson of the Univeristy of Illinois at Urbana-Champaign for collection of single-crystal X-ray data sets, and Dr. Christophe Auriel of Université de Pau in France for his help in the solution of the crystal structure $K_{1.5}Dy_2Cu_{2.5}Te_5$. This research was supported by National Science Foundation under Grant DMR-9319196. We thank the J.D. and C.T. MacArthur foundations for a fellowship granted to S.L.

Supporting Information Available: Tables of crystallographic data and anisotropic thermal factors (2 pages) and listings of structure factors (10 pages) for the three copper tellurides. Ordering information is given on any current masthead page.

CM970700B

(16) (a) $NaCu_3Te_2$: Klepp, K. O. *Z. Naturforsch.* **1987**, *B42*, 130. (b) KCu_3Te_2; Savelsberg, G.; Schaefer, H. *Mater. Res. Bull.* **1981**, *16*, 1291. (c) $C_{58}H_{46}Cu_2N_6S_4{\cdot}2(CH_3NO_2)$: Potts, K. T.; Keshavarz-K, M.; Tham, F. S.; Abruna, H. D.; Arana, C. *Inorg. Chem.* **1993**, *32*, 4450.

(17) (a) Pyykkö, P. *Chem. Rev.* **1997**, *97*, 597. (b) Mehrotra, P. K.; Hoffmann, R. *Inorg. Chem.* **1978**, *17*, 2187.